

1 **Neurocranial development of the coelacanth and the evolution of the**  
2 **sarcopterygian head**

3  
4 Hugo Dutel<sup>1,2</sup>, Manon Galland<sup>3</sup>, Paul Tafforeau<sup>4</sup>, John A. Long<sup>5</sup>, Michael J. Fagan<sup>1</sup>,  
5 Philippe Janvier<sup>6</sup>, Anthony Herrel<sup>7</sup>, Mathieu D. Santin<sup>8</sup>, Gaël Clément<sup>6</sup>, Marc Herbin<sup>7</sup>

6  
7 <sup>1</sup>School of Engineering and Computer Science, Medical and Biological Engineering  
8 Research Group, University of Hull, Hull, HU6 7RX, UK.

9 <sup>2</sup>School of Earth Sciences, University of Bristol, Bristol, BS8 1TQ, UK.

10 <sup>3</sup>UMR 7206 (Sorbonne Université-MNHN-CNRS), Éco-Anthropologie et Ethnobiologie,  
11 Département Homme et Environnement, Muséum national d'Histoire naturelle, Paris  
12 75005, France.

13 <sup>4</sup>European Synchrotron Radiation Facility, F-38043, Grenoble, France.

14 <sup>5</sup>College of Science and Engineering, Flinders University, Adelaide, SA 5001,  
15 Australia.

16 <sup>6</sup>UMR 7207 (Sorbonne Université-MNHN-CNRS), CR2P : Centre de Recherche en  
17 Paléontologie, Département Origines et Évolution, Muséum national d'Histoire  
18 naturelle, Paris 75005, France.

19 <sup>7</sup>UMR 7179 (MNHN-CNRS) MECADEV, Département Adaptations du Vivant, Muséum  
20 national d'Histoire naturelle, Paris 75005, France.

21 <sup>8</sup>Centre for NeuroImaging Research, Institut du Cerveau et de la Moelle épinière,  
22 Inserm U 1127, CNRS UMR 7225, Sorbonne Université, F-75013, Paris France.

23  
24 **The neurocranium of sarcopterygian fishes was originally divided into an**  
25 **anterior (ethmosphenoid) and posterior (otoccipital) portion by an intracranial**  
26 **joint, and underwent major changes in its overall geometry before fusing into a**  
27 **single unit in lungfishes and early tetrapods<sup>1</sup>. Although the pattern of these**  
28 **changes is well documented, the developmental mechanisms underpinning the**  
29 **variation in neurocranial form and its associated soft tissues during the**  
30 **evolution of sarcopterygian fishes remain poorly understood. The coelacanth**  
31 ***Latimeria* is the only living vertebrate retaining an intracranial joint and has a**  
32 **tiny brain lying deeply posterior within the otoccipital portion<sup>2,3</sup>. Despite its**  
33 **evolutionary significance, the development of the neurocranium of this**  
34 **ovoviviparous fish is virtually unknown. Here, we investigate the ontogeny of**  
35 **the neurocranium and brain in *Latimeria chalumnae* based on conventional and**

1 **synchrotron X-ray microtomography, as well as magnetic resonance imaging**  
2 **performed on the most extensive growth series available for this species. We**  
3 **describe the neurocranium at its earliest developmental stage and the major**  
4 **changes it undergoes during ontogeny. Changes in the neurocranium are**  
5 **associated with an extreme reduction in the relative size of the brain along with**  
6 **an enlargement of the notochord. The notochordal development appears to have**  
7 **a major impact on the surrounding cranial components, and might underpin the**  
8 **formation of the intracranial joint. Our results shed light on the interplay between**  
9 **the neurocranium and its adjacent soft tissues during the development of**  
10 ***Latimeria*, and provide important insights into the developmental mechanisms**  
11 **underpinning neurocranial diversity during the evolution of sarcopterygian**  
12 **fishes.**

13         Although the coelacanth *Latimeria* has been studied extensively since its  
14 discovery 80 years ago<sup>4</sup>, most aspects of its cranial development still remain  
15 unknown<sup>2</sup>. This lack of knowledge is largely due to the scarcity of embryonic material  
16 and, until recently, the absence of efficient non-invasive methods to study the internal  
17 anatomy of these rare specimens. Here, we digitalized five specimens (see  
18 Supplementary Information for methods) ranging from the prenatal to postnatal  
19 development of this ovoviviparous species: a small foetus (5 cm total length, TL), a  
20 pup with yolk sac (P1, 30.5 cm TL), a pup without yolk sac (P2, 35.6 cm TL), a juvenile  
21 (42 cm TL), and an adult (A1, 132 cm TL) (Fig. 1). To the best of our knowledge, these  
22 specimens represent the most complete growth series currently available for this  
23 species.

24         In the foetus, the neurocranium is already divided into two portions at the level  
25 of the ventral fissure and the intracranial joint (Figs 1,2, Extended Figure 1). The  
26 individualisation of the two divisions of the neurocranium thus occurs earlier, probably  
27 during the early embryonic development. The ethmosphenoid division of the  
28 neurocranium is much narrower and slightly longer than the otoccipital one, and  
29 lengthens during prenatal development (Figs 2,3, Extended Figure 1). The trabeculae  
30 extend anteroventrally to the notochord, and delimit the open hypophyseal fossa. They  
31 fuse anteriorly as a narrow trabeculae communis (Fig. 2, Extended Figure 1 and 2).  
32 Posteriorly, the ethmosphenoid portion develops around the anterior notochordal tip in  
33 the foetus, whereas it lies entirely anterior to the notochord in latter stages. The  
34 notochord penetrates the ethmosphenoid portion posterodorsal to the trabeculae, and  
35 terminates posterior to the hypophysis, the foramina for the internal carotids, the

1 pituitary vein, and the oculomotor nerve (Figs 2,3, Extended Figure 1). At this level,  
2 the neurocranium shows a marked curvature under the cephalic flexure.  
3 Topographically, this region is similar to what is observed in other gnathostomes, and  
4 interpreted as deriving from the orbital cartilage<sup>5-7</sup>. A shallow dorsum sellae separates  
5 the hypophyseal fossa and the large basicranial fenestra. In the otoccipital portion, the  
6 parachordals are widely separated and extend anteriorly as a short otic shelf. The otic  
7 region is shallow, the commissura prefacialis is open, as is the metotic fissure in the  
8 posterior wall of the otic capsule (Fig. 2, Extended Figure 1).

9         The configuration of the neurocranium and brain observed in the foetus is, to  
10 our knowledge, unique compared to other gnathostomes<sup>6,7</sup>. The endocranial cavity  
11 reaches the neurocranial floor in the ethmosphenoid portion, but continues dorsally to  
12 the notochordal canal in the otoccipital portion (Figs 2,3, Extended Figures 1 and 2).  
13 The cerebellum and mesencephalon straddles the anterior and posterior divisions, and  
14 are positioned dorsally to the forebrain and the ethmosphenoid portion. The short pila  
15 antotica meets the orbital cartilage ventral to the mesencephalon, and the trochlear  
16 nerve emerges above the eyes (Fig 2, Extended Figure 1). Dorsally, the neurocranium  
17 is largely incomplete around the cerebellum and the mesencephalon, and the taenia  
18 marginalis posterior fails to reach the orbital cartilage. Later during the prenatal  
19 development, the endocranium of the ethmosphenoid portion moves dorsally as a  
20 narrow internasal septum develops such that P1 presents a tropibasic neurocranium  
21 (Fig. 3, Extended Figure 2). The ethmoidal region is proportionally shorter in the foetus  
22 compared to the adult as the cavity for the rostral organ is not yet formed (Figs 2,3,  
23 Extended Figure 1). Only from P1 onwards is the cavity for the rostral organ separated  
24 from the endocranial cavity, which is steeply depressed in its anterior portion (Fig. 3).  
25 The expansion of the rostral organ remodels the ethmoid region and displaces the  
26 ethmoidal articulation from the postnasal wall in the foetus, and to the lateral side of  
27 the nasal capsules in other stages (Figs 2,3, Extended Figure 1).

28         The reduction in the relative size of the brain (Extended Table 1) and changes  
29 in its shape (Fig. 3, Extended Figure 3) are associated with a progressive displacement  
30 towards the otoccipital portion. In the foetus (Figs 2,3, Extended Figures 1-3), the brain  
31 straddles the intracranial joint and the telencephalon reaches the nasal capsules. In  
32 P1, P2, and the juvenile (Fig. 3, Extended Figures 3 and 4), the brain represents about  
33 11% of the endocranial volume. The telecephalon still spans the intracranial joint but  
34 the mesencephalon is restricted to the otoccipital portion. The confinement of the brain  
35 within the otoccipital portion occurs only during the postnatal development (Fig. 3,

1 Extended Figure 3). In the adult (Fig. 3, Extended Figure 3), the entire brain is  
2 restricted to the otoccipital portion, and represents 1% of the endocranial volume, as  
3 reported previously<sup>2,3</sup>. In the foetus, the brain is curved ventrally and the cephalic  
4 flexure is less pronounced than in other groups, as the rhombencephalon and the  
5 mesencephalon develop far dorsal to the forebrain (Figs 2,3, Extended Figures 1-3).  
6 This configuration is retained in P1, but not in P2, in which the brain straightens (Fig.  
7 3, Extended Figure 3). In the foetus, the hypophysis and the hypothalamus are  
8 positioned vertically below the mesencephalon. They are displaced towards the  
9 telencephalon during ontogeny, as a long hypophyseal duct elongates and extends  
10 into a deep hypophyseal fossa (Fig. 3, Extended Figure 3). The endocranium of the  
11 foetus is proportionally broader than in other stages, having short olfactory canals,  
12 divergent olfactory capsules, and a short hypophyseal fossa (Fig. 3). These  
13 characteristics can be regarded as plesiomorphic, and are shared by stem-  
14 osteichthyans<sup>8</sup>, early sharks and placoderms<sup>9</sup>, and the tetrapodomorph fish  
15 *Tungsenia*<sup>10</sup>. From P1 onwards (Fig. 3), the endocranium shows the typical shape  
16 observed in sarcopterygians<sup>9,11,12</sup>, with long olfactory canals, a narrow cavity spanning  
17 above the interorbital septum, and a deep hypophyseal fossa extending  
18 anteroventrally. Beyond the mismatch between the brain and the endocranium in  
19 adults, the changes in the position, relative size, and shape of the brain are reflected  
20 by the endocranium throughout the ontogeny of *Latimeria*.

21 The size of the notochord is similar to that of the rhombencephalon in the foetus  
22 (Figs 2,3, Extended Figure 1), and is proportionally larger compared to that of other  
23 taxa at a similar developmental stage<sup>6</sup>. Only the rostral notochordal tip is markedly  
24 reduced and finishes behind the hypophysis, which likely reflects its initial anterior  
25 position. The notochordal foramen in the ethmosphenoid portion is lost in later stages  
26 as the basisphenoid ossifies, but retained in adult stem-sarcopterygians<sup>13,14</sup>. In  
27 contrast to the brain, the notochord undergoes a proportionally greater degree of  
28 expansion than the endocranial cavity in later stages (Fig. 3, Extended Table 1). Thus,  
29 the expansion of the notochord likely starts during the embryonic phase of  
30 development, and its position remains almost unchanged throughout ontogeny.

31 Our results illuminate, for the first time, the development of the neurocranial  
32 structures in *Latimeria*. The neurocranium is divided into two portions in the earliest  
33 observed stage of ontogeny, but remains topographically conservative relative to that  
34 of other gnathostomes<sup>5-7,15</sup>. The ethmosphenoid portion is entirely anterior to the  
35 notochord in adults, but develops partly in the prechordal domain as it includes the

1 orbital cartilage and the rostral notochordal tip. As such, the intracranial joint is not  
2 coincident with the limit between the mesoderm-derived and the neural crested-  
3 derived neurocranium<sup>15–17</sup>, but posterior to it. In addition to a complete division of the  
4 neurocranium, the *Latimeria* foetus shows a unique combination of developmental  
5 characteristics. The prechordal region is proportionally much narrower than in embryos  
6 of lungfishes<sup>6,18</sup>, *Polypterus*, *Amia*, and amphibians<sup>6,7</sup>, in which the trabeculae are  
7 widely separated and in line with the parachordals. In these taxa, the brain straightens  
8 as it folds extensively during the early ontogeny, allowing its encapsulation within the  
9 neurocranium<sup>19</sup>. The configuration of the brain in the *Latimeria* foetus derives from this  
10 general pattern and, together with the deep dorsum sellae<sup>20</sup>, probably results from the  
11 enlargement of the notochord. The development of the latter is profoundly altered in  
12 *Latimeria* compared to other living vertebrates (Fig. 4), in which the notochord always  
13 reduces and retracts from the hypophyseal region relatively early in development<sup>6,7,21</sup>.

14         The development of the notochord observed in *Latimeria* appears to impact the  
15 adjacent tissues, and might underpin the complete division of the neurocranium. By  
16 remaining in an anterior position and expanding in early ontogeny, the notochord  
17 probably separates the parachordals broadly and restricts the narrow trabecular plate  
18 and the orbital cartilage anteriorly, thus hindering their fusion. As the notochord  
19 expands, the hindbrain and midbrain are displaced dorsal to the ethmosphenoid  
20 portion, and their volume likely affects the patterning of the adjacent neurocranial roof.  
21 Hence, we suggest that the intracranial joint likely resulted from the novel configuration  
22 of the brain as imposed by the notochord. Accordingly, the complete division of the  
23 braincase is always associated with a very large notochord in contact with the dorsum  
24 sellae, a deep hypophyseal fossa, and a relatively narrow hypophyseal region of the  
25 braincase with respect to the otoccipital division<sup>1,9,22</sup>. The modulation of the growth  
26 trajectories of the brain and notochord might also allow the persistence of a ventral  
27 fissure when the intracranial joint is consolidated, as in the stem lungfish  
28 *Youngolepis*<sup>23</sup>.

29         A discrepancy between the brain and the endocranial cavity exists in various  
30 fishes<sup>24,25</sup>, but the magnitude of the mismatch observed in adult *Latimeria* is, to our  
31 knowledge, unequalled among living vertebrates. In living gnathostomes, the forebrain  
32 lengthen anterior to the eyes above the trabecular plate, as the hypophysis expends  
33 posteriorly<sup>26</sup> (Fig. 4). This early developmental pattern appears to be shared by  
34 *Latimeria*, given the position of the forebrain in the foetus and its proportions in adults  
35 (Fig. 2, Extended Figure 3). However, the notochord later fills up the space behind the

1 hyophyseal fossa that is otherwise occupied by the brain in other taxa (Fig. 4). The  
2 dramatic expansion of the notochord thus likely causes a major spatial packing  
3 constraint on the brain and restricts the growth of the hypophyseal and orbital regions  
4 anteriorly, which might drive the allometric growth and elongation of the brain. The  
5 similarities between the endocranium of *Latimeria* pups and those of stem-  
6 sarcopterygians<sup>9,12–14</sup> suggest that this developmental pattern is ancestral to the group,  
7 whereas brain shape appears to match that of the endocranium in fossil  
8 actinopterygians and stem-osteichthyans<sup>8,11</sup>. Accordingly, the ventral expansion of the  
9 brain<sup>27</sup> and the higher brain-to-body mass ratio in extant lungfishes<sup>28</sup> and tetrapods<sup>19</sup>  
10 (Fig. 4) might have been permitted by the progressive reduction and displacement of  
11 the notochord posterior to the otic capsule during the respective evolution of these  
12 lineages<sup>22,29</sup>. However, we hypothesize that the displacement of the entire brain into  
13 the otoccipital portion that occurs relatively late during the development of *Latimeria*  
14 might result from biomechanical constraints linked to the intracranial joint<sup>30</sup>.

## 16 **Methods Summary**

17 All the specimens were obtained from public natural history collections (see  
18 Supplementary Information for a detailed description of the specimens). The foetus,  
19 the pups, and the juvenile were imaged using propagation phase contrast X-ray  
20 synchrotron microtomography on the beamline ID19 at the ESRF, Grenoble, France.  
21 The adult specimen was imaged using a conventional microtomograph (Phoenix  
22 vltomelx 240 L, General Electric) at the AST-RX CT-scan facility of the MNHN, UMS  
23 2700 CNRS-MNHN, Paris, France. All the scanning parameters are provided in  
24 Supplementary Information. MRI acquisitions were performed with a Bruker Biospec  
25 System (Bruker, Germany), at the Institut du Cerveau et de la Moelle épinière, Paris,  
26 France. For all specimens, segmentation was performed using MIMICS 15 and 17  
27 (Materialise, Leuven, Belgium), and three-dimensional models were rendered under  
28 Cinema 4D Studio (Maxon Computer, Friedrichsdorf, Germany).

## 30 **References**

- 31 1. Ahlberg, P. E., Clack, J. A. & Luksevics, E. Rapid braincase evolution between  
32 *Panderichthys* and the earliest tetrapods. *Nature* **381**, 61–64 (1996).
- 33 2. Anthony, J. & Robineau, D. Sur quelques caractères juvéniles de *Latimeria*  
34 *chalumnae* Smith (Pisces, Crossopterygii Coelacanthidae). *C. R. Acad. Sci.,*  
35 *Ser. D* **283**, 1739–1742 (1976).

- 1 3. Millot, J. & Anthony, J. *Anatomie de Latimeria chalumnae. II. Système Nerveux*  
2 *et Organes des Sens.* (Centre National de la Recherche Scientifique, 1965).
- 3 4. Smith, J. L. B. A living fish of the Mesozoic type. *Nature* **143**, 455–456 (1939).
- 4 5. Kuratani, S. Development of the Chondrocranium of the Loggerhead Turtle,  
5 *Caretta caretta*. *Zoolog. Sci.* **16**, 803–818 (1999).
- 6 6. de Beer, G. R. *The development of the vertebrate skull.* (University of Chicago  
7 Press, 1938).
- 8 7. Goodrich, E. S. *Studies on the structure and development of vertebrates.* **1**,  
9 (Macmillan, 1930).
- 10 8. Clement, A. M. *et al.* Neurocranial anatomy of an enigmatic Early Devonian fish  
11 sheds light on early osteichthyan evolution. *Elife* **7**, e34349 (2018).
- 12 9. Janvier, P. *Early Vertebrates.* (Clarendon Press, 1996).
- 13 10. Lu, J. *et al.* The earliest known stem-tetrapod from the Lower Devonian of China.  
14 *Nat. Commun.* **3**, 1160 (2012).
- 15 11. Giles, S. & Friedman, M. Virtual reconstruction of endocast anatomy in early  
16 ray-finned fishes (Osteichthyes, Actinopterygii). *J. Paleontol.* **88**, 636–651  
17 (2014).
- 18 12. Lu, J. *et al.* A Devonian predatory fish provides insights into the early evolution  
19 of modern sarcopterygians. *Sci. Adv.* **2**, (2016).
- 20 13. Yu, X. A new porolepiform-like fish, *Psarolepis romeri*, gen. et sp. nov.  
21 (Sarcopterygii, Osteichthyes) from the Lower Devonian of Yunnan, China. *J.*  
22 *Vertebr. Paleontol.* **18**, 261–274 (1998).
- 23 14. Andrews, S. M., Long, J. A., Ahlberg, P. E., Barwick, R. E. & Campbell, K. The  
24 structure of the sarcopterygian *Onychodus jandemarrai* n. sp. from Gogo,  
25 Western Australia: with a functional interpretation of the skeleton. *Trans. R. Soc.*  
26 *Edinburgh-Earth Sci.* **96**, 197–307 (2006).
- 27 15. Kuratani, S., Adachi, N., Wada, N., Oisi, Y. & Sugahara, F. Developmental and  
28 evolutionary significance of the mandibular arch and prechordal/premandibular  
29 cranium in vertebrates: revising the heterotopy scenario of gnathostome jaw  
30 evolution. *J. Anat.* **222**, 41–55 (2012).
- 31 16. Kuratani, S. The neural crest and origin of the neurocranium in vertebrates.  
32 *Genesis* **56**, e23213 (2018).
- 33 17. Clack, J. A. in *Major events in early vertebrate evolution* (ed. Ahlberg, P. E.)  
34 392–505 (Systematics Association Symposium Volume, 2001).
- 35 18. Kemp, A. Ontogeny of the skull of the Australian lungfish *Neoceratodus forsteri*

- 1 (Osteichthyes: Dipnoi). *J. Zool.* **248**, 97–137 (1999).
- 2 19. Dubbeldam, J. L. *et al.* *The Central Nervous System of Vertebrates 1–3*, 2214  
3 (1998).
- 4 20. Maisey, J. G. in *Major Events in Early Vertebrate Evolution* (ed. Ahlberg, P. E.)  
5 263–288 (Taylor and Francis, 2001).
- 6 21. Kemp, A. Early development of neural tissues and mesenchyme in the  
7 Australian lungfish *Neoceratodus forsteri* (Osteichthyes: Dipnoi). *J. Zool.* **250**,  
8 347–372 (2000).
- 9 22. Ahlberg, P. E., Clack, J. A., Lukševičs, E., Blom, H. & Zupiņš, I. *Ventastega*  
10 *curonica* and the origin of tetrapod morphology. *Nature* **453**, 1199–1204 (2008).
- 11 23. Mee-Mann, C. The braincase of *Youngolepis*, a Lower Devonian  
12 crossopterygian from Yunnan, South-Western China. *Department of Geology,*  
13 *University of Stockholm, and Section of Palaeozoology, Swedish Museum of*  
14 *Natural History* (1982).
- 15 24. Pradel, A. *et al.* Skull and brain of a 300-million-year-old chimaeroid fish  
16 revealed by synchrotron holotomography. *Proc. Natl. Acad. Sci. USA* **106**,  
17 5224–5228 (2009).
- 18 25. Kruska, D. C. T. The Brain of the Basking Shark (*Cetorhinus maximus*). *Brain.*  
19 *Behav. Evol.* **32**, 353–363 (1988).
- 20 26. Dupret, V., Sanchez, S., Goujet, D., Tafforeau, P. & Ahlberg, P. E. A primitive  
21 placoderm sheds light on the origin of the jawed vertebrate face. *Nature* **507**,  
22 500–503 (2014).
- 23 27. Clement, A. M., Nysjö, J., Strand, R. & Ahlberg, P. E. Brain-endocast  
24 relationship in the Australian lungfish, *Neoceratodus forsteri*, elucidated from  
25 tomographic data (Sarcopterygii: Dipnoi). *PLoS One* **10**, e0141277 (2015).
- 26 28. Northcutt, R. G., Neary, T. J. & Senn, D. G. Observations on the brain of the  
27 coelacanth *Latimeria chalumnae*: External anatomy and quantitative analysis.  
28 *J. Morphol.* **155**, 181–192 (1978).
- 29 29. Clement, A. M. & Ahlberg, P. E. The first virtual cranial endocast of a lungfish  
30 (Sarcopterygii: Dipnoi). *PLoS One* **9**, e113898 (2014).
- 31 30. Dutel, H., Herbin, M., Clément, G. & Herrel, A. Bite force in the extant coelacanth  
32 *Latimeria*: The role of the intracranial joint and the basicranial muscle. *Curr. Biol.*  
33 **25**, 1228–1233 (2015).

34

35 **Supplementary Information** is available in the online version of the paper.

1

## 2 **Acknowledgement**

3 We thank R. Bills and A. Paterson (SAIAB, Grahamstown, South Africa) for the loan of  
4 the foetus, as well as D. Neumann (ZSM, Munich, Germany) for the loan of P2. We  
5 thank M. Garcia Sanz for  $\mu$ CT-scanning of the adult specimen at “AST-RX, plate-forme  
6 d'accès scientifique à la tomographie à rayons X” in the “UMS 2700 Outils et Méthodes  
7 de Systématique intégrative CNRS-MNHN”. We thank the ESRF for granting beam  
8 time to H.D. on ID19 for performing the PPC-SR $\mu$ CT acquisitions (Proposal EC-1023).  
9 We thank C. Bens and A. Verguin of the Collections de Pièces anatomiques en Fluides  
10 at the MNHN for their help. We thank É. Heude (MNHN, Paris, France) and P. Gueriau  
11 (University of Lausanne, Lausanne, Switzerland) for their valuable comments and  
12 input on an earlier version of the draft. This work was supported by a grant from Agence  
13 Nationale de la Recherche under the LabEx ANR-10-LABX-0003-BCDiv, in the  
14 program “Investissements d'avenir” n\u0001 ANR-11-IDEX-0004-02. H.D. was  
15 supported by a BBSRC grant (BB/M008525/1).

16

## 17 **Author contributions**

18 H.D., G.C., M.H., A.H. and P.J. designed the research. H.D. and P.T. made the PPC-  
19 SR $\mu$ CT acquisitions. H.D., G.C. and M.H. made the conventional microtomographical  
20 acquisitions with the assistance of the local staff. M.D.S. made the MRI acquisitions.  
21 H.D. segmented the scans and made the 3D rendering of all the developmental stages,  
22 with the assistance of M.G. J.A.L. provided fossil material for comparative study and  
23 provided input for the discussion. M.J.F and A.H. provided input for the results and  
24 discussion. H.D. wrote the manuscript, made the figures and the scientific illustrations.  
25 All the other authors provided critical comments and were involved in the writing of the  
26 manuscript. All the authors accepted the final version of the manuscript.

27

## 28 **Author Information**

29 The PPC-SR $\mu$ CT acquisitions are available online at <http://paleo.esrf.eu>. Surface files  
30 are deposited online at **Dryad link to be inserted here**. The authors declare no  
31 competing financial interests. Correspondence and request material should be  
32 addressed to H.D. (h.dutel@bristol.ac.uk).

33

34 **Figure 1** The development of the living coelacanth *L. chalumnae*. **a**, Growth series  
35 gathered for this study. **b**, overall anterolateral view of the skull of the foetus.

1

2 **Figure 2** Comparison of the neurocranium between a foetus (left column) and adult  
3 (right column) of *L. chalumnae*. **a**, right lateral view. **b**, ventral view. **c**, right lateral view  
4 of the neurocranium virtually cut open along the midsagittal plane. ap, antotic process;  
5 Boc, basioccipital; bf, basicranial fenestra; Bs, basisphenoid; ce, cerebellum; cf,  
6 cephalic flexure; cpf, commissura prefacialis; cro, cavity for the rostral organ; die,  
7 diencephalon; ds, dorsum sellae; Eth, ethmoid bone; eth, ethmoid cartilage; eth.a,  
8 ethmoidal articulation; eth.p, ethmoidal process; fm, foramen magnum; fic, foramen for  
9 internal carotid artery; fpv, foramen for the pituitary vein; hf, hypophyseal fossa; ins,  
10 internasal septum; ios, interorbital septum; mes, mesencephalon; mf, metotic fissure;  
11 n, notochord; nac, nasal capsule; nc, notochoral canal; oc, orbital cartilage; oro,  
12 opening for the rostral organ; os, otic shelf; otc, otic capsule; pa, pila antotica; Par,  
13 parasphenoid; pc, parachordal plate; Pro, prootic; rho, rhombencephalon; sc,  
14 supraorbital cartilage; ssc, supraorbital sensory canal; t, trabeculae; tc, trabeculae  
15 communis; tel, telencephalon; tm, taenia marginalis; top, transverse otic process; vf,  
16 ventral fissure; I, olfactory nerve; II, optic nerve; III, oculomotor nerve; IV, trochlear  
17 nerve or foramen for; V1, ophthalmic branch of the trigeminal nerve; V23,  
18 maxillomandibular branch of the trigeminal nerve VI; abducens nerve; VII, facial nerve;  
19 IX, glossopharyngeal nerve or foramen for; X, vagus nerve.

20

21 **Figure 3** Endocranium and brain morphology in *L. chalumnae* growth series. The  
22 foetus (**a**), pup 1 (**b**), pup 2 (**c**), juvenile (**d**), and the adult (**e**) in right lateral (left column)  
23 and dorsal (right column) views. Grey portions in the juvenile (**d**) were reconstructed  
24 based on pup 2 (**c**). The rostral organ was not reconstructed in (**d**) since it was  
25 destroyed. cf, cephalic flexure; die, diencephalon; ds, dorsum sellae; h, hypophysis;  
26 hp, hypothalamus; ij, intracranial joint; nac, nasal capsule; mes, mesencephalon; olc,  
27 olfactory canal; rho, rhombencephalon; tel, telencephalon; I, olfactory nerve; II, optic  
28 nerve; III, oculomotor nerve; IV, trochlear nerve; V1, ophthalmic branch of the  
29 trigeminal nerve; V23, maxillomandibular branch of the trigeminal nerve VI; abducens  
30 nerve; VII, facial nerve; IX, glossopharyngeal nerve; X, vagus nerve.

31

32 **Figure 4** Neurocranium of selected extant osteichthyan fishes and tetrapod. The  
33 endocrania are shown in left lateral view and aligned on the foramina for the optic (II)  
34 and vagus (X) nerves. The neurocranium of sarcopterygians is ancestrally divided into  
35 two portions by the intracranial joint and the ventral fissure, and its consolidation into

1 a single unit occurred independently in lungfishes and tetrapods. Note the position and  
2 relative size of the brain and notochord, the configuration of the brain, and the  
3 orientation of the hypophysis in *Latimeria* with respect to other taxa. *Neoceratodus* is  
4 redrawn from ref. 19 and ref. 27. Subadult *Polypterus* and *Tylototriton* are drawn from  
5 PPC-SR $\mu$ CT acquisitions, and the adult *Latimeria* is drawn based on Fig. 3.

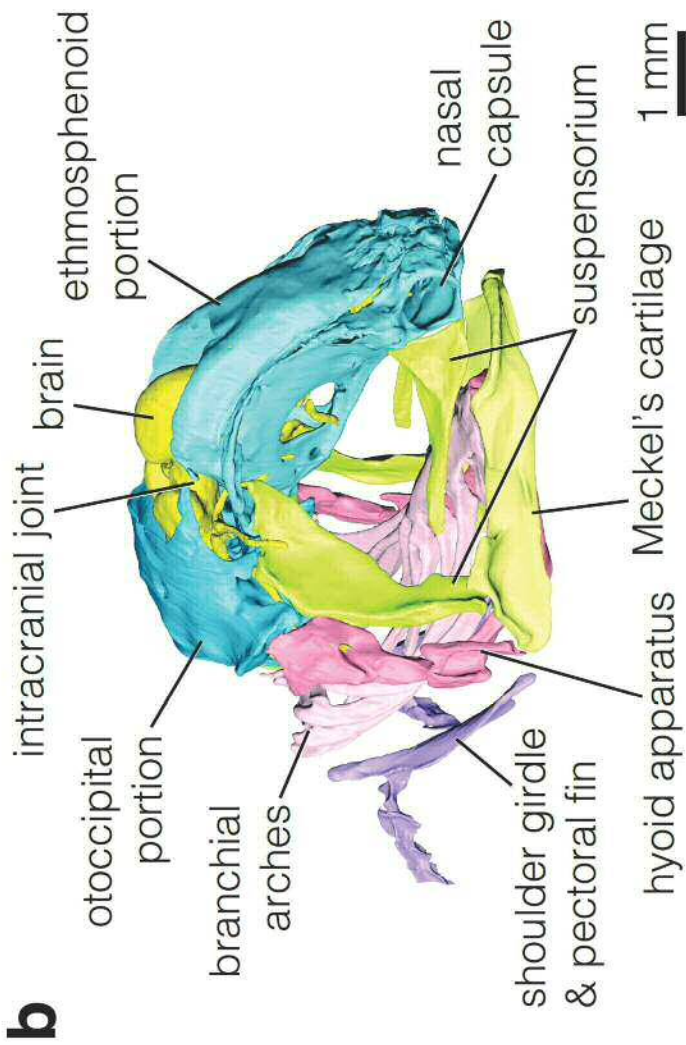
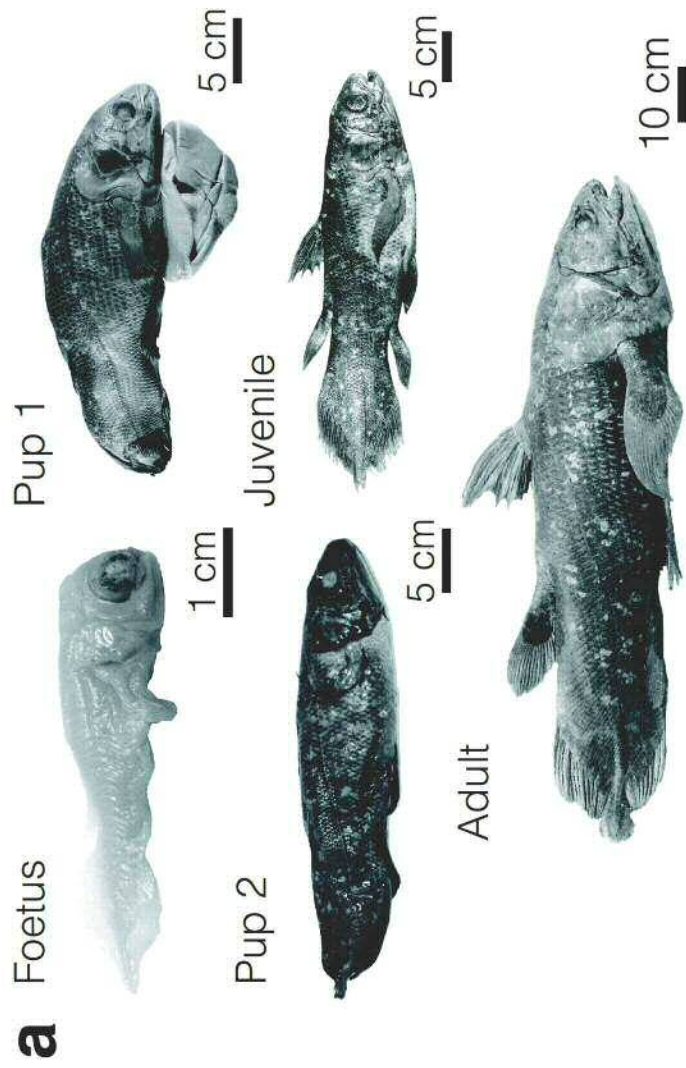
6  
7 **Extended Figure 1** The foetus of *L. chalumnae*. **a-b**, the neurocranium in right  
8 anterolateral view, with the ethmosphenoid portion virtually cut open along the mid-  
9 sagittal plane in **(b)**. **c-d**, dorsal view of the neurocranium with the roof of the otoccipital  
10 portion virtually cut open. The brain is shown in position **(c)**, and was digitally removed  
11 **(d)** to show the underlying neurocranial structures. **e**, posterior view of the  
12 ethmosphenoid portion. **f**, posterior view of the otoccipital portion.

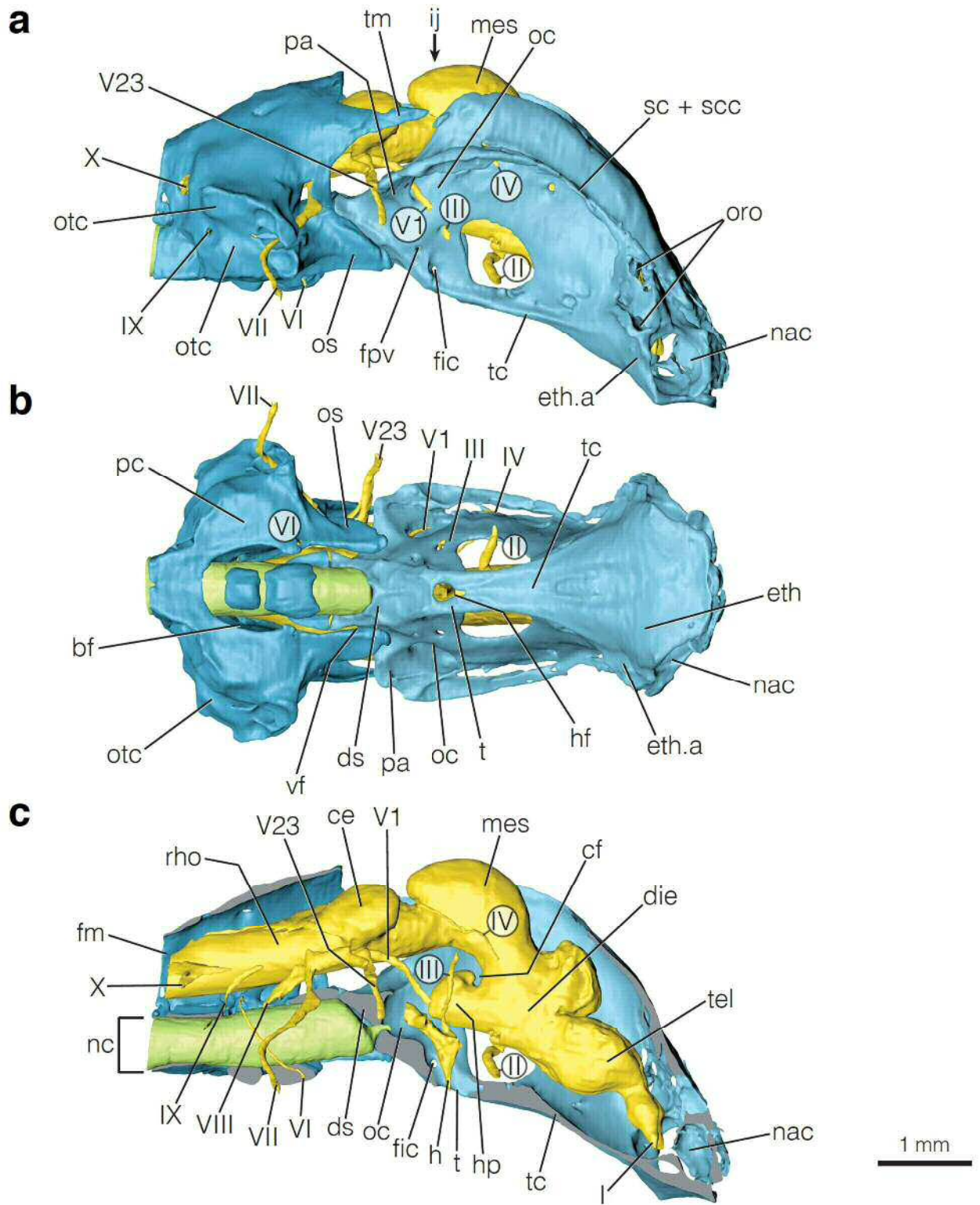
13  
14 **Extended Figure 2** Coronal sections obtained from PPC-SR $\mu$ CT acquisition along the  
15 head of the foetus (left column) and pup 1 (right column) of *L. chalumnae*. **a**, section  
16 at the level of the orbital foramen. **b**, section at the level of the hypophyseal fossa. **c**,  
17 section at the level of the basisphenoid-palatoquadrate joint. **d**, section at the level of  
18 the inner ear. All the scanning parameters are provided in Supplementary Information.

19  
20 **Extended Figure 3** The brain of *L. chalumnae* in the foetus **(a)**, pup 1 **(b)**, pup 2 **(c)**,  
21 and the adult **(d)** in right lateral view (left) and dorsal (right) views. The brain of the  
22 juvenile is not displayed as it was extracted from the endocranium, and not imaged *in*  
23 *situ*.

24  
25 **Extended Figure 4** The dissection of the juvenile (MNHN C79) performed in 1974 at  
26 the Muséum national d'Histoire naturelle, Paris, France. As in earlier developmental  
27 stages, the brain spans the intracranial joint (indicated by the needle) in the juvenile.  
28 Scale in centimetres.

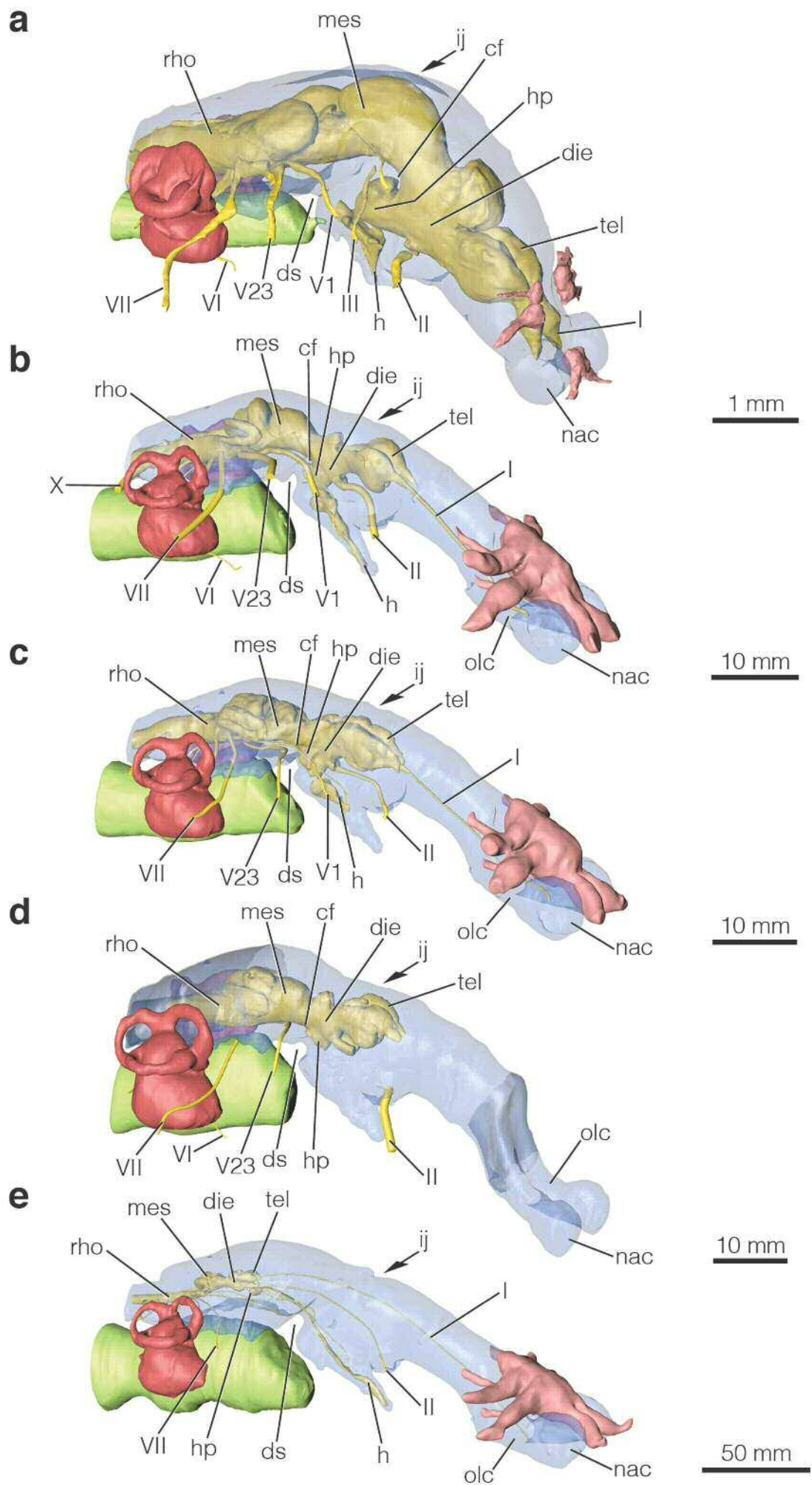
29  
30 **Extended Table 1** Morphometric measurements of the notochord, brain and  
31 endocranial cavity. All volumes are in mm<sup>3</sup>. Asterisk indicates structures for which the  
32 missing portions have been digitally restored in the juvenile before making the  
33 measurements.



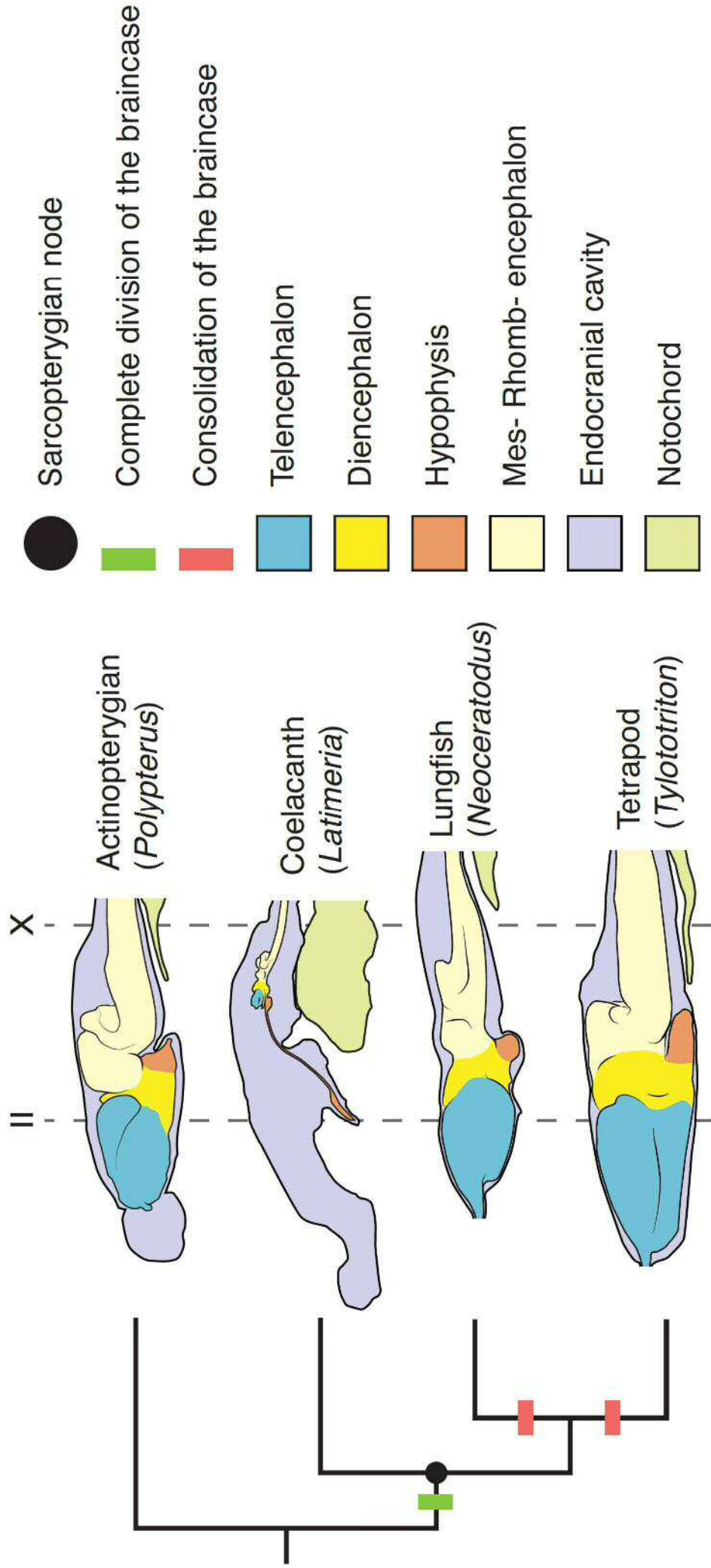


otoccipital portion
  ethmosphenoid portion
  brain
  notochord

1 mm



endocranial cavity
  brain, cranial nerves
  primordium of the rostral organ (foetus), cavity for the rostral organ (other stages)
  inner ear
  notochord



# Supplementary Information for Neurocranial development of the coelacanth and the evolution of the sarcopterygian head

Hugo Dutel, Manon Galland, Paul Tafforeau, John A. Long, Michael J. Fagan, Philippe Janvier, Anthony Herrel, Mathieu D. Santin, Gaël Clément, Marc Herbin

## Table of contents

I.	Additional results and discussion .....	1
I.1	Morphometric measurements and effect of the fixatives .....	1
I.3	Additional anatomical observations and comparisons .....	4
II.	Supplementary references .....	9

## I. Additional results and discussion

### I.1 Morphometric measurements and effect of the fixatives

To further compare the growth of the brain, the notochord, and the endocranial cavity we measured the volume of these structures (Extended Data Table 1). Brain volume was measured from the portion laying just posteriorly to the foramen for the vagus nerve to the tip of the telencephalon. Regarding the juvenile brain, the portion of the rhombencephalon cut during the dissection was restored with a cylinder spanning up to the back of the vagus nerve, which allowed us to estimate the volume of the juvenile brain within the endocranial cavity. The same posterior limit was taken for measuring the volume of the endocranial cavity. These measurements show that the brain reaches almost a quarter of its final size at the end of the prenatal development (Extended Data Table 1). The volume of the notochord was measured from the edge of basioccipital (i.e. the posteriormost point of the neurocranium) to its anterior tip in contact with the basisphenoid. The absolute size of the brain is higher than that of the notochord only in the fetus.

Fixation prevents tissues decay, but also inevitably alters the shape and size of the tissues to different degrees. Therefore, a key question concerning our observations is whether the formalin fixation could have induced the important discrepancy observed between the volume of the brain and that of the endocranial cavity in the different development stages. The change in volume and shape depends on the type of fixative used. Formalin and

glutaraldehyde can induce a slight swelling of the tissues, followed by a shrinkage phase before stabilization in the volume (Vickerton et al. 2013). By contrast, ethanol produces a more important and continuous shrinkage of the tissues (Vickerton et al. 2013). Based on the affine registration of MRI acquisitions, Schulz et al. (2011) reported that *in situ* formalin (10%) fixation causes an anisotropic shrinkage of 8.1% in the volume of human brains over a period of 70 days. The different regions of the brain do not deform in the same manner, and maximal strain fields were quantified in the peripheral layers of the brain (Schulz et al. 2011). When dissected and immersed in 10% formaldehyde in PBS during 28 days, the average shrinkage rate for skeletal muscle, cardiac muscles and cerebellum is slightly higher (around 12%, fig. 3 in (Vickerton et al. 2013) that what would be expected when fixed *in situ* (Vickerton et al. 2013). However, there is a close correspondence between the measurements in brain volume and cortical thickness made with MRI on formalin fixed (10%) and live rhesus macaques (*Macaca mulatta*) (Calabrese et al. 2015). Taking the volume of the endocranial cavity as a reference, the shrinkage rate would have been of 87% in P2, and 99% in the adult for the brain to obtain its measured volume. The experimental studies published hence indicate that, despite having an effect on the tissues, the formalin fixation cannot result in a sufficient shrinkage for the brain to have the condition observed in the coelacanth specimens. Moreover, all specimens underwent fixation likely causing a similar degree of shrinkage in all specimens.

The limited impact of the fixation on the tissues is also supported by the comparison of the formalin fixed pups and the juvenile. The latter was frozen at -18°C about two hours after death and sent to Paris for study in 1974 (Anthony & Robineau 1976; Nulens et al. 2011). The specimen was still frozen upon arrival at the MNHN (Anthony & Robineau 1976; Nulens et al. 2011), and the skull roof was removed to observe the brain *in situ* (Extended Data Fig. 5) the day following the defrosting of the specimen. We observed a close correspondence in the position and relative size of the brain between this specimen and the pups fixed in formalin, which further supports that the fixation had little effect on the tissues and allows for a gross anatomical study of these specimens.

Regarding the adults, our calculation of the ratio between the volume of the brain and that of the endocranial cavity is very similar to the estimates that were made fifty three years ago by Millot and Anthony (1965) on specimens recently fixed in formalin. This suggests that formalin has little long-term effects on the tissues, or if there are any, they might be balanced by the intraspecific variability and/or the method employed to perform the measurements. In addition, the measurements of brain volumes, and the ratio between the brain and endocranial volume are similar in adult specimens, despite the fact that the adult was stained with a solution of 5% phosphomolybdic acid in 70% ethanol (Dutel et al. 2013). Finally, reports indicate that

the specimens were rapidly (within a few hours) formalin fixed or frozen after being captured in Comoro islands (Millot & Anthony 1965; Nulens et al. 2011), thus indicating that the decay and alteration of the tissues after death was limited.

The fixation with ethanol has been reported to cause more shrinkage in tissues than formalin (Vickerton et al. 2013). Indeed, ethanol fixes the tissues by causing its dehydration, and the degree of shrinkage of the tissues is proportional to the concentration in ethanol of the solution (Boyde & Maconnachie 1980). Therefore, the brain volume we measured in the fetus, which was fixed in ethanol, likely represents a greater underestimation than that for the other developmental stages. Yet, the topographic relationship between the brain and the endocranial cavity, as exemplified by the position of the foramina of the cranial nerves is consistent with what can be observed in other taxa. Thus, this suggest that the shrinkage that could have been caused by the fixation did not alter dramatically the position of the brain within the endocranial cavity. As such, we think that the potential bias in the brain volume measured in the fetus does not change our results pertaining to the understanding of the relationships between the brain and the braincase during coelacanth development.

In the juvenile specimen, the extraction of the brain from the endocranial cavity has altered its shape and volume. When compared with the photograph showing the brain *in situ* within the endocranial cavity (Extended Data Fig. 5), the brain reconstructed appears to have the auriculae cerebelli and the telencephalon squashed along the body of the brain (Fig. 3, Extended Data Fig. 3). In addition, the digital reconstruction of the regions of the braincase destroyed during the dissection might also introduce biases in the measurements made on this developmental stage. Although probably underestimated, the ratio between the brain and endocranial volume matches the values found for P1 and P2 and provide insight into the position and relative volume of the brain in free-swimming juveniles.

As a conclusion, the fixative used to preserve the specimens represents a potential source of error in the measurements of the brain volume. However, experimental studies and comparison with unfixed specimens show that the important discrepancy between the brain and endocranial volumes is not artefactual, and rather results from the negative allometric growth of the brain relative to the endocranial cavity. In addition, the correspondence between measurements made on formalin-fixed specimen more than 50 years ago and ours indicates that such natural history collections are suitable for being used in gross-anatomical studies.

### I.3 Additional anatomical observations and comparisons

#### External morphology of the neurocranium

Until now, the development of the extant coelacanth *Latimeria* was known only through the description of the head morphology of a juvenile (Anthony & Robineau 1976), and the description of the cranial nerves of a prepartum specimen (Northcutt & Bemis 1993). Our study hence represents the first comprehensive description of the development of the brain and neurocranium in one of the two species of living coelacanth.

The overall dimensions of the neurocranium vary during the ontogeny of *Latimeria* (Figs. 2,3, Extended Data Figs. 1-3). The ethmosphenoid portion is markedly longer and narrower than the otoccipital portion in the adult than in the fetus (Fig. 3, Extended Data Fig. 3). The ethmosphenoid portion of the braincase is much broader in the fetus than in adult *Latimeria*, and the ethmoid region markedly shorter in length. During the development, the short and broad ethmoid region observed in the fetus narrows and expands posteriorly and anteriorly, so that the overall proportions of the ethmosphenoid portion in adult *Latimeria* is similar to what is observed in *Eusthenopteron* (Downs et al. 2008; Jarvik 1980) (Fig 3, Extended Data Fig. 3). The neurocranial dimensions of these taxa differ from those of more basal tetrapodomorph and sarcopterygian fishes, but more closely matches the elpistostegalian *Panderichthys* (Ahlberg et al. 1996). The trends towards a longer ethmosphenoid division of the neurocranium is also observed in the coelacanth lineage: the neurocranium of early coelacanths *Miguashaia* (Cloutier 1996), *Diplocercides* (Forey 1998; Stensiö 1937), *Gavinia* (Long 1999), and *Euporosteus* (Stensiö 1937; Zhu et al. 2012), and *Styloichthys* (which was interpreted as either a basal actinistian [Friedman 2007] or stem sarcopterygian [King et al. 2017; Qiao et al. 2016]) shares similar neurocranial dimensions with the fetus of *Latimeria*, as well as a short ethmoid region, large orbits, the presence of a metotic fissure, and a buccohypophyseal canal opening on the parasphenoid. The fetus of *Latimeria* (Figs. 1, 2) is strikingly similar to the fossil embryo of the Triassic coelacanth *Rhaboderma* (Schultze 1972), and later prenatal stages show similar proportions of their neurocranium with the juvenile specimens of the Devonian coelacanth *Serenichthys* (Gess & Coates 2015). Unfortunately, the preservation of these specimens does not allow a detailed observation of the external and internal neurocranial anatomy. With the exception of the recently described genus *Foreyia* (Cavin et al. 2017), Mesozoic coelacanths (Carnier Fragoso et al. 2018; Cavin et al. 2016; Dutel et al. 2012, 2015; Forey 1998; Maisey 1986) are similar to adult specimens of *Latimeria*, and share with it a longer and narrower ethmosphenoid portion, and the absence of the an opening for the buccohypophyseal canal on the parasphenoid. The variation in

neurocranial form is exemplified in Mawsoniidae, in which the relative length ethmosphenoid portion is longer than in *Latimeria* (Carnier Fragoso et al. 2018; Dutel et al. 2015; Maisey 1986). The trend towards a slender and elongate snout appears to be associated with an increase of the overall body size in fossil coelacanth (Dutel et al. 2012, 2015; Maisey 1986) and during the ontogeny of *Latimeria*. The congruence between this evolutionary trend and the developmental pattern observed in *Latimeria* suggests that allometry likely represents a strong driver of variation of skull shape during coelacanth evolution.

The broad ethmoid region of the fetus also differs from the adult in the position of the articulation with the palate. In the fetus of *Latimeria*, as well as in stem-sarcopterygians (Yu 1998) and onychodonts (Andrews et al. 2006), the ethmoid articulation lies posterior to the postnasal wall. By contrast, this articulation is located in a fossa ventrolateral to the nostrils and formed by the lateral ethmoid and the ascending wing of the parasphenoid in the pups, juvenile, and adult *Latimeria* (Millot and Anthony 1958), as well as in fossil coelacanth (Friedman 2007). Our observation of the developmental stages of *Latimeria* shows that the displacement of the ethmoid articulation is related to the shallowing and anteroposterior extension of the ethmoid region, which might be constrained by the expansion of the rostral organ and its lateral canals (Fig. 3, Extended Data Fig. 3).

The otoccipital portion is shorter and broader in the fetus than in the adult. In ventral view, the otoccipital region of the fetus shows a short otic shelf, and much narrower basicranial fenestra where the notochord passes through. With respect to other neurocranial structures, the notochord is much smaller in the fetus than in the other stages. The commissura prefacialis is open in the fetus, and that the cartilaginous rods that forms the descending process for the postparietal in adults is still separated from the otic shelf (Extended Data Fig. 1). The posterior wall of the otic region narrows markedly, and is perforated by the large metotic fontanelle, which spans ventrally to the foramen for the glossopharyngeal and vagus nerves (Extended Data Fig. 1). The otic process that carries the articulatory facets for the hyomandibula, which position is lower in the fetus than in the adult. The walls of the endocranial cavity are pierced by two large openings, through which the acoustic and glossopharyngeal nerves are passing.

The fetus and adult *Latimeria* specimens show marked differences in the position of the foramen for the cranial nerves and blood vessels. In the fetus, the foramen for the internal carotid artery and the foramen for the pituitary vein are located ventrally and posteroventrally to the foramen for the oculomotor nerve, respectively (Fig. 2, Extended Data Figs. 1, 3). In the adult, the foramen for the pituitary vein and the foramen for the internal carotid artery are displaced anteroventrally to the foramen for the oculomotor nerve (Extended Data Fig. 3). Because of the reduction of the optic foramen and its dorsal displacement during ontogeny,

the foramen for the internal carotid artery lies ventrally to the optic foramen in the adult (Extended Data Fig. 3). The foramen for the trochlear nerve opens more anteriorly with respect to the foramen for the maxillary branch of the trigeminal nerve in the fetus. The relative position of the foramina on the ethmosphenoid portion of the skull in the fetus is hence similar to what can be observed in *Psarolepis* (Yu 1998), as well as in the Devonian coelacanths *Diplocercides* (Stensiö 1937, 1963) and *Euporoosteus* (Forey 1998; Stensiö 1937), and in the stem-tetrapodomorph *Tungsenia* (Lu et al. 2012). With respect to the otoccipital portion of the neurocranium, the foramen for the facial nerve and the jugular canal are located more anteriorly to the foramen for the vagus nerve in the fetus. During *Latimeria* development, the position of the foramen for the vagus nerve, the jugular canal and the foramen for the glossopharyngeal nerve appear to be displaced posteriorly closer to each other. Comparison with fossil coelacanths is however difficult, as the otoccipital portion is largely made of cartilage in Mesozoic coelacanths (Forey 1998) and poorly or not preserved in Devonian coelacanths.

The *Latimeria* fetus shares with stem sarcopterygians the presence of a foramen in the middle of the notochordal pit, through which an extension of the notochord passes to reach to hypophyseal fossa (Fig. 2, Extended Data Fig. 1). Such a foramen is also observed in the stem-sarcopterygian *Psarolepis* (Yu 1998) and in *Onychodus* (Andrews et al. 2006). This condition is not observed in later development stages of *Latimeria*, and might reflect the anteriormost position occupied by the notochord during the embryonic development.

## Endocast

The *Latimeria* fetus presents short olfactory tract canals and olfactory capsules that are widely separated relative to the midline, and are positioned close to the hypophyseal fossa (Fig. 3, Extended Data Fig. 3). By contrast, other developmental stages show longer olfactory tract canals and closed olfactory capsules that are positioned further away from the hypophyseal fossa (Fig. 3, Extended Data Fig. 3). The morphology of the nasal capsules in *Latimeria* fetus is also observed in placoderms (Stensiö 1963; Young 1979), in the chondrichthyan *Cladodoides* (Maisey 2005), in the stem-osteichthyan *Ligulalepis* (Clement et al. 2018), in early actinopterygians, in the stem-sarcopterygians *Psarolepis* (Qiao et al. 2011), *Quigmenodus* (Lu et al. 2016) and in the tetrapodomorph *Tungsenia* (Lu et al. 2012). The endocast of the pups, juvenile, and adult markedly differ from that of the fetus in having a deep depression in its anterior aspect, which was called “ensellure rostrale” by Millot and Anthony (1965). This depression goes along the ventral margin of the cavity for the rostral organ, which is more developed in these stages than in the fetus. As such, the development of a coelacanth-

specific neurosensory organ likely constrains the shape of the ethmoid region of the neurocranium.

The ethmosphenoid region of the endocast is much broader in the fetus than in other developmental stages (Fig. 3, Extended Data Fig. 3). The ethmosphenoid region of the endocast is about the same width than the otoccipital portion, with the broader point located at the level of the foramen for the trochlear nerve (Fig. 3, Extended Data Figs. 1, 3). Ventrally, the endocranial cavity extends to the floor of the braincase with a very short hypophyseal fossa which expands posterodorsally as a well-developed swelling perforated by the foramen for the pituitary vein (Fig. 2, Extended Data Figs. 1, 2). This recess in the endocast houses the hypothalamus and the pars intermedia of the hypophysis, that are positioned ventral to the mesencephalon in the fetus (Fig. 3, Extended Data Fig. 3). The configuration of the hypophyseal region in the fetus recalls that of *Ligulalepis* (Clement et al. 2018), and *Tungsenia* (Lu et al. 2012). By contrast, the hypophyseal region in the pups resemble more to what is observed in onychodonts (Lu et al. 2016).

Contrary to what is observed in other living taxa, the otoccipital division of *Latimeria* endocranium is positioned very dorsally by respect to its anterior counterpart. Accordingly, the mesencephalon and rhombencephalon are positioned dorsally to the forebrain, which is packed within the ethmosphenoid division of the braincase in the fetus. The endocranium of *Latimeria* fetus is flexed ventrally at the level of the cephalic flexure, which is positioned above the hypophyseal fossa. The configuration of the brain observed in *Latimeria* fetus is markedly different from what is observed in living chondrichthyans, actinopterygians, lungfishes and amphibians (Nieuwenhuys et al. 1998). In these taxa, the brain straightens as it extensively folds during the early ontogeny, so that the rhombencephalon, the mesencephalon and the forebrain develop merely in line, and encapsulated within the endocranium. In addition, the hypothalamus and the hypophysis are displaced posteroventrally to the diencephalon and span horizontally below the mesencephalon as a deep cephalic flexure develops in these taxa (Nieuwenhuys et al. 1998). This developmental pattern is associated with the reduction of the notochord, and its displacement towards the otic capsule (de Beer 1938; Goodrich 1930) (Fig. 4). By contrast, the notochord is enlarged and ends close to the hypophyseal fossa in the fetus of *Latimeria* (Figs. 2, 3, Extended Data Figs. 1, 3) and later developmental stages. As such, the neurocranial floor in the otoccipital portion is displaced dorsally to the neurocranial floor in the ethmosphenoid portion because of the volume occupied by the underlying notochord. We suggest that the alteration of the developmental trajectory of the notochord in *Latimeria* results in the unusual configuration of the brain and neurocranium observed in the fetus.

In dorsal view, the endocast of the pups, the juvenile and the adult is much narrower at the level of the ethmosphenoid region than in the otoccipital region (Fig. 3, Extended Data Fig. 3). The endocranial cavity shows a marked notch at the level of the intracranial joint, but widens laterally at the level of the foramen for the trochlear nerve, just dorsal to the level of the hypophyseal fossa. This widening of the endocranial cavity is more marked in P1, P2 and the juvenile than in the adults, as this portion of the braincase houses the telencephalic hemispheres and the narrower diencephalon spans the intracranial joint (Fig. 3, Extended Data Fig. 3). Such a swelling of the endocast is also observed the early actinopterygian *Mimipiscis* (Giles & Friedman 2014) and in the stem-osteichthyan *Ligulalepis* (Clement et al. 2018). In the latter, the short hypophyseal fossa is tilted posteriorly, ventral to the widest region of the endocranium which is interpreted as housing the mesencephalon and the cerebellum. Our observations support this interpretation and show that the marked swellings of the endocranial wall in *Latimeria* accommodate larger brain regions, despite the fact that the brain form does not closely matches that of the endocranial cavity. The width of the endocast is more regular in the ethmosphenoid portion of the adult *Latimeria* (Extended Data Fig. 3), and reminiscent of the condition observed in *Eusthenopteron* (Jarvik 1980; Stensiö 1963). In this taxa, the brain was reconstructed as filling the entire endocranial cavity, with the forebrain reaching the olfactory canals (Jarvik 1980; Stensiö 1963). Yet, we think that the previous neuroanatomical reconstructions in *Eusthenopteron* will ought to be re-evaluated based on the new developmental data available for *Latimeria*.

The otoccipital portion of the endocast presents less variation across the developmental stages of *Latimeria* than the ethmosphenoid portion. In dorsal view, the otoccipital portion of the endocast is slightly wider than the ethmosphenoid in the fetus, the widest point being located at mid-length, at the level of the auricula cerebelli and anteriorly to the emergence of the facial nerve (Fig. 3, Extended Data Fig. 1). The foetal endocast narrows and reduces in height progressively in its posterior half, before broadening at the level of the foramen for the vagus nerve. The upper half of the inner ear is positioned in the recess made by the braincase. The endocast of the otoccipital portion is deeper than the notochord, and the ventral aspect of the sacculus lies at the level of the ventral side of the notochord (Extended Data Fig. 3). In the fetus, the otoccipital portion of the endocast only houses the posterior portion of the mesencephalon and the rhombencephalon (Fig. 3, Extended Data Figs. 1, 3). In P1, P2, and the juvenile, the endocast of the otoccipital portion is slenderer and shallower (Fig. 3, Extended Data Fig. 3). In the pups, the roof the endocast is markedly flexed to accommodate the cerebellum, whereas it is slightly curved in the adult.

## II. Supplementary references

- Ahlberg PE, Clack JA, Luksevics E. 1996. Rapid braincase evolution between *Panderichthys* and the earliest tetrapods. *Nature*. 381(6577):61–64
- Andrews SM, Long JA, Ahlberg PE, Barwick RE, Campbell K. 2006. The structure of the sarcopterygian *Onychodus jandemarrai* n. sp. from Gogo, Western Australia: with a functional interpretation of the skeleton. *Trans. R. Soc. Edinburgh-Earth Sci.* 96(03):197–307
- Anthony J, Robineau D. 1976. Sur quelques caractères juvéniles de *Latimeria chalumnae* Smith (Pisces, Crossopterygii Coelacanthidae). *C. R. Acad. Sci., Ser. D.* 283:1739–42
- Boyde A, Maconnachie E. 1980. Treatment with lithium salts reduces ethanol dehydration shrinkage of glutaraldehyde fixed tissue. *Histochemistry*. 66(2):181–87
- Calabrese E, Badea A, Coe CL, Lubach GR, Shi Y, et al. 2015. A diffusion tensor MRI atlas of the postmortem rhesus macaque brain. *Neuroimage*. 117:408–16
- Carnier Fragoso LG, Brito P, Yabumoto Y. 2018. *Axelrodichthys araripensis* Maisey, 1986 revisited. *Hist. Biol.* 1–23
- Cavin L, Mennecart B, Obrist C, Costeur L, Furrer H. 2017. Heterochronic evolution explains novel body shape in a Triassic coelacanth from Switzerland. *Sci. Rep.* 1:13695
- Cavin L, Valentin X, Garcia G. 2016. A new mawsoniid coelacanth (Actinistia) from the Upper Cretaceous of Southern France. *Cretac. Res.* 62:65–73
- Clement AM, King B, Giles S, Choo B, Ahlberg PE, et al. 2018. Neurocranial anatomy of an enigmatic Early Devonian fish sheds light on early osteichthyan evolution. *Elife*. 7:e34349
- Cloutier R. 1996. The primitive actinistian *Miguashaia bureaui* Schultze (Sarcopterygii). In *Devonian Fishes and Plants of Miguasha, Québec, Canada*, eds. H-P Schultze, R Cloutier, pp. 227–47. München: Verlag Dr. Friedrich Pfeil
- de Beer GR. 1938. *The Development of the Vertebrate Skull*. Chicago: University of Chicago Press
- Downs JP, Daeschler EB, Jenkins FA, Shubin NH. 2008. The cranial endoskeleton of *Tiktaalik roseae*. *Nature*. 455:925–29
- Dutel H, Herbin M, Clément G. 2015. First occurrence of a mawsoniid coelacanth in the Early Jurassic of Europe. *J. Vertebr. Paleontol.* 35(3):e929581
- Dutel H, Herrel A, Clément G, Herbin M. 2013. A re-evaluation of the anatomy of the jaw-closing system in the extant coelacanth *Latimeria chalumnae*. *Naturwissenschaften*. 100:1007–22
- Dutel H, Maisey JG, Schwimmer DR, Janvier P, Herbin M, Clément G. 2012. The giant

- Cretaceous coelacanth (Actinistia, Sarcopterygii) *Megalocoelacanthus dobiei* Schwimmer, Stewart & Williams, 1994, and its bearing on Latimerioidei interrelationships. *PLoS One*. 7(11):e49911
- Forey PL. 1998. *History of the Coelacanth Fishes*. London: Chapman and Hall
- Friedman M. 2007. *Styloichthys* as the oldest coelacanth: implications for early osteichthyan interrelationships. *J. Syst. Palaeontol.* 5(3):289–343
- Gess RW, Coates MI. 2015. Fossil juvenile coelacanths from the Devonian of South Africa shed light on the order of character acquisition in actinistians. *Zool. J. Linn. Soc.* 175(2):360–83
- Giles S, Friedman M. 2014. Virtual reconstruction of endocast anatomy in early ray-finned fishes (Osteichthyes, Actinopterygii). *J. Paleontol.* 88(4):636–51
- Goodrich ES. 1930. *Studies on the Structure and Development of Vertebrates*, Vol. 1. London NV - 2: Macmillan
- Jarvik E. 1980. *Basic Structure and Evolution of Vertebrates*, Vol. 1. London: Academic Press
- King B, Qiao T, Lee MSY, Zhu M, Long JA. 2017. Bayesian morphological clock methods resurrect placoderm monophyly and reveal rapid early evolution in jawed vertebrates. *Syst. Biol.* 66(4):499–516
- Long JA. 1999. A new genus of fossil coelacanths (Osteichthyes: Coelacanthiformes) from the Middle Devonian of southeastern Australia. *Rec. West. Aust. Museum.* 57:37–53
- Lu J, Zhu M, Ahlberg PE, Qiao T, Zhu Y, et al. 2016. A Devonian predatory fish provides insights into the early evolution of modern sarcopterygians. *Sci. Adv.* 2(6):e1600154
- Lu J, Zhu M, Long JA, Zhao W, Senden TJ, et al. 2012. The earliest known stem-tetrapod from the Lower Devonian of China. *Nat. Commun.* 3:1160
- Maisey JG. 1986. Coelacanths from the Lower Cretaceous of Brazil. *Am. Museum Novit.* 2866:1–30
- Maisey JG. 2005. Braincase of the Upper Devonian Shark *Cladodoides wildungensis* (Chondrichthyes, Elasmobranchii), with observations on the braincase in early Chondrichthyans. *Bull. Am. Museum Nat. Hist.* 288:1
- Millot J, Anthony J. 1958. *Anatomie de Latimeria Chalumnae. I. Squelette et muscles*. Paris: Centre National de la Recherche Scientifique
- Millot J, Anthony J. 1965. *Anatomie de Latimeria Chalumnae. II. Système Nerveux et Organes Des Sens*. Paris: Centre National de la Recherche Scientifique
- Nieuwenhuys R, ten Donkelaar HJ, Nicholson C (eds) 1998. *The Central Nervous System of Vertebrates*, Vols. 1–3. Berlin, Heidelberg: Springer-Verlag
- Northcutt RG, Bemis WE. 1993. Cranial nerves of the coelacanth, *Latimeria chalumnae*

- [Osteichthyes: Sarcopterygii: Actinistia], and comparisons with other craniata. *Brain Behav. Evol.* 42:1–76
- Nulens R, Scott L, Herbin M. 2011. An updated inventory of all known specimens of the coelacanth *Latimeria* spp. *Smithiana Publ. Aquat. Biodivers.* 3:1–52
- Qiao T, King B, Long JA, Ahlberg PE, Zhu M. 2016. Early gnathostome phylogeny revisited: Multiple method consensus. *PLoS One.* 11(9):e0163157
- Qiao T, Lu J, Zhu M, Long JA. 2011. Cranial anatomy of a primitive osteichthyan *Psarolepis* based on high-resolution computed tomography. *J. Vertebr. Paleontol.* 31(Supplement to 3):177
- Schultze H-P. 1972. Early growth stages in coelacanth fishes. *Nature.* 236:90–91
- Schulz G, Crooijmans HJA, Germann M, Scheffler K, Müller-Gerbl M, Müller B. 2011. Three-dimensional strain fields in human brain resulting from formalin fixation. *J. Neurosci. Methods.* 202(1):17–27
- Stensiö EA. 1937. On the Devonian coelacanthids of Germany with special reference to the dermal skeleton. *K. Sven. Vetenskapsakademiens Handl.* 3(16):1–56
- Stensiö EA. 1963. The brain and the cranial nerves in fossil, lower craniate vertebrates. *Skr. Utg. av Det Nor. Videnskaps-Akademi i Oslo, Mat.-Naturv. Klasse. Ny Ser. 13.* 120
- Vickerton P, Jarvis J, Jeffery N. 2013. Concentration-dependent specimen shrinkage in iodine-enhanced microCT. *J. Anat.* 223(2):185–93
- Young GC. 1979. New information on the structure and relationships of *Buchanosteus* (Placodermi: Euarthrodira) from the Early Devonian of New South Wales. *Zool. J. Linn. Soc.* 66(4):309–52
- Yu X. 1998. A new porolepiform-like fish, *Psarolepis romeri*, gen. et sp. nov. (Sarcopterygii, Osteichthyes) from the Lower Devonian of Yunnan, China. *J. Vertebr. Paleontol.* 18(2):261–74
- Zhu M, Yu X, Lu J, Qiao T, Zhao W, Jia L. 2012. Earliest known coelacanth skull extends the range of anatomically modern coelacanths to the Early Devonian. *Nat. Commun.* 3:772.